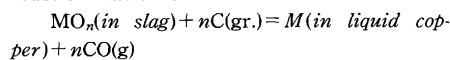


Fundamentals of High Temperature Processes

Thermodynamic properties of the MgO-BO_{1.5} binary system at 1723 K

X. HUANG *et al.*

To determine the thermodynamic properties of the MgO-BO_{1.5} binary system, the following reaction was used:



where MO_n represents MgO or BO_{1.5}.

The activity coefficients of boron and magnesium in liquid copper were first determined by equilibrating pure liquid B₂O₃ or pure solid MgO with liquid copper under controlled CO partial pressure in a graphite crucible at 1723 K:

$$\ln \gamma_B = 0.82 + 2.81x_B,$$

$$\ln \gamma_{Mg} = -1.22(x_B \leq 0.106, x_{Mg} \leq 0.0013)$$

The thermodynamic properties of MgO and BO_{1.5} in MgO-BO_{1.5} binary slag at 1723 K were determined as a function of composition by equilibrating the MgO-BO_{1.5} slag with liquid copper under CO atmosphere. In addition, the interaction parameter (ϵ_{Mg}^B) in the Cu-B-Mg alloy was determined to be -100 at 1723 K.

Liquid phase boundaries at 1873 K in the ternary CaO-Al₂O₃-MO_x (MO_x: MgO, ZrO₂) and CaO-SiO₂-MO_x (MO_x: TiO₂, MgO, Al₂O₃) systems

H. SAKAI *et al.*

The liquid phase boundaries in the CaO-Al₂O₃-MgO, CaO-Al₂O₃-ZrO₂, CaO-SiO₂-TiO₂, CaO-SiO₂-MgO and CaO-SiO₂-Al₂O₃ ternary slags were determined at 1873 K by using a slag-crucible (CaO, MgO, Al₂O₃ and ZrO₂-11mol% CaO) equilibration technique. The equilibrium phase at crucible-slag interface was determined by a microprobe analysis.

Nitride capacities in the CaO-base ternary slags at 1873 K

H. SAKAI *et al.*

Nitride capacities ($C_N = (\text{mass}\% \text{ N}) P_{O_2}^{3/4} / P_{N_2}^{1/2}$) in the CaO-Al₂O₃-MgO(ZrO₂) and CaO-SiO₂-MgO(TiO_x) ternary slags were measured at 1873 K by a gas-slag equilibration technique, using a Mo, Al₂O₃ or MgO crucible under controlled partial pressures of oxygen ($\log(P_{O_2}/\text{Pa}) = -11 \sim -14$) and nitrogen ($P_{N_2} = 0.9\text{Pa}$). The C_N values increased with increasing the contents of nitride former oxides. The C_N values in the CaO-AlO_{1.5}-MO_x (MO_x = MgO, SiO₂, ZrO₂, TiO_x) slags at $X_{CaO}/X_{AlO_{1.5}} = 0.4 \sim 0.7$ increased in the order of MgO < SiO₂ < ZrO₂ < TiO_x and those in the CaO-SiO₂-MO_x (MO_x = MgO, AlO_{1.5}, TiO_x) slags at $X_{CaO}/X_{SiO_2} = 1.0 \sim 1.5$ increased in the order of MgO < AlO_{1.5} < TiO_x at a given MO_x content.

Ironmaking and Reduction

Estimation of effective thermal diffusivity of porous solid using data for image processing

H. NISHIOKA *et al.*

Many equations for the estimation of effective thermal diffusivity of porous solid were proposed previously. However, those equations do not always represent the correct effective thermal diffusivity of the porous solid, because of the complexity of the pore structure of the porous solid. Therefore, in this work, effective thermal diffusivity of porous iron was estimated by computer simulation of heat transfer in the porous iron using data of microstructure of the sample. The measurement of the effective thermal diffusivity of the sample by Laser Flash method was also carried out. The estimated results agreed well with the observed data.

Simultaneous behavior of pulverized coal char combustion and fine iron oxide reduction by injecting the mixture of coal char and iron oxide

S.-M. KANG *et al.*

The present study has been carried out to investigate the simultaneous behavior of combustion of 'pulverized coal char' (described as 'char' afterwards in this paper), and of reduction of fine iron ore using a laboratory scale tube furnace.

Experimental results show that apparent combustion rate of char is not affected by the ore/char mole ratio simultaneously injected. The reaction rate constant of char was not changed with changing wustite/char injection ratio. On the other hand, the rate constant of char increased proportionally with an increase of hematite/char injection ratio. This implies that hematite behaves as an effective oxygen source for char combustion.

The main reduction mechanism of fine wustite injected is found to be the direct reduction between molten wustite and unburnt carbon. Similarly, for the case of fine hematites, the direct reduction between molten magnetite thermally decomposed from hematite and solid carbon entrained into the droplet is the main reduction mechanism.

It was observed that the reduction degree of fine iron oxides mainly depends on the specific combustion heat (kJ/g-ore) which is defined as the ratio of combustion heat of char to the feeding rate of fine iron oxide.

Carbon monoxide reduction and accompanying swelling of iron oxide compacts

M. I. NASR *et al.*

Pure Fe₂O₃ compacts were fired at 1373 K for one hour then reduced with CO at 973-1373 K. Reduction was followed up by means of weight-loss technique whereas volume change was measured by displacement method. The

structure of the fired and reduced compacts was examined by reflected light microscope while the different phases were identified by X-ray diffraction technique. These measurements together with kinetic data were correlated for better understanding the gas-solid reaction mechanisms and the accompanying swelling phenomenon. A highest swelling value of 176 % was obtained for compacts completely reduced at 1173 K whereas a maximum swelling of 224 % was obtained for compacts 90 % reduced at the same temperature. At all reduction temperatures swelling increased with the increase in reduction extent up to 90 % where a maximum swelling value was obtained followed by a small decrease in swelling when compacts were completely reduced. Excessive swelling was attributed to the carbon in metallic iron and/or iron carbide formed and their reactions with oxygen forming CO and/or CO₂. A mechanism of disintegration of iron grains and swelling of the compacts has been proposed and correlated with reduction conditions.

Forming Processing and Construction

Microstructure and corrosion behaviour of Ni-P laser surface alloys

M. C. GARCIA-ALONSO *et al.*

Two different coat thickness electroless Ni-P deposits on mild steel were laser treated at two different laser scanning rates. To generate a coated surface of various square centimetres, five laser tracks were realized overlapping 50 % of each other. The Ni-P coated samples treated in this way were microstructurally characterized and its corrosion behaviour on 0.1M Na₂SO₄ solution was determined. As a consequence of the laser interaction, a dendritic solidification microstructure was obtained for all the Ni-P coatings-initially amorphous-tested independently of its coat thickness or the laser treatment conditions. The low corrosion resistance of laser treated Ni-P coatings of 45 μm coat thickness makes them not suitable for technological applications. However, laser treatment of Ni-P coated samples with the maximum coat thickness tested (180 μm) enhances its corrosion resistance in the medium studied.

Effect of microstructure for base steel on Fe-Zn alloy growth during galvanizing of interstitial free steel

T. NAKAMORI *et al.*

The effect of the microstructure of the base steel on the formation and growth behavior of intermetallics on interstitial free steel during galvanizing under various processing conditions (substrate entry temperature, Al content in galvanizing bath) was investigated from the viewpoint of the surface morphology of the intermetallics. In addition, the surface mor-

phology of galvanized coating was also examined.

The dependency of Fe-Zn intermetallics growth behavior on the crystal orientation of the base steel was observed clearly in galvanizing in 0.10 mass% or less Al bath, especially at low entry temperatures. In general, ξ crystals are precipitated orderly on (111) α , whereas those are precipitated disorderly on (001) α and (101) α at the outset of the formation of Fe-Zn intermetallics, and the growth rate of Fe-Zn intermetallics on (001) α and (101) α is larger than that on (111) α .

As an exception, the formation of Fe-Zn intermetallics on (001) α and (101) α at the outset of Fe-Zn interaction is suppressed at the entry temperature of 673 K in 0.10 mass% Al bath, although the clump of orderly precipitated ξ is formed on (111) α .

The growth of Fe-Zn intermetallics during galvanizing also depends on crystallographic orientation of α Fe grain of the base steel, being retarded on (111) α . A large α Fe grain with (111) α on the surface is thought to cause a concave portion on the galvanized surface.

Consequently, it is thought that the formation and growth behavior of Fe-Zn intermetallics on IF steel is affected not only by α Fe grain boundary but also by crystallographic orientation of α Fe grain of the base steel.

Microstructure

Effects of lattice defect behaviors on pre-precipitation stages of γ' and γ'' phases in a Ni-base superalloy

K. NAKAI et al.

The preprecipitation processes of γ' and γ'' intermetallic phases and their effects on age hardening processes in an alloy 718 have been examined in relation to both solution treatment and aging temperature. The results were analyzed mainly in terms of the behaviors of quenched-in excess vacancies as well as constituent atoms of γ' and γ'' precipitates, Ti, Al and/or Nb, around as-grown dislocations. Dislocation dipoles linked to each other formed remarkably during the early stage of aging in the specimen solution-treated at higher temperature. The dislocation dipoles disappeared almost simultaneously with the initiation of γ' and/or γ'' precipitations, and eventually age hardening started. In the specimen solution-treated at the lowest temperature the most rapid age hardening occurred due to the γ' and/or γ'' intragranular precipitations under the adequate migration of the constituent atoms without the formation of the dislocation dipoles. The initiation of precipitation hardening in the early stage of aging was confirmed to depend greatly on the behavior of the constituent atoms associated with the excess vacancy migration around as-grown dislocations. It is concluded that the formation of dislocation dipoles suppresses the γ' and γ'' precipitations due to the segregation of the

constituent atoms to the dislocation dipoles, and the mechanisms of the segregation and dissipation of the constituent atoms around the dislocation dipoles are discussed.

Grain growth predictions in microalloyed steels

P. A. MANOHAR et al.

Empirical models for grain growth predictions are briefly reviewed. It is demonstrated that such models are inadequate for quantitative prediction of austenite grain growth during reheating of as-cast microstructures in microalloyed steels. This inadequacy is mainly attributable to the inability of empirical models to account for abnormal grain growth. Basic principles of grain growth are therefore revisited in an attempt to develop a mathematical model which can account for abnormal grain growth. Such a model has been developed for Ti: N balanced microalloyed steels and is presented here. It is shown that quantitative predictions of austenite grain growth generated from this model fit well with experimental grain growth data obtained during reheating of as-cast slabs of Ti, Ti+Nb as well as Ti+Nb+Mo containing microalloyed steels.

Modeling of transformation behavior and compositional partitioning in TRIP steel

T. MINOTE et al.

Transformation behavior and compositional partitioning in TRIP (Transformation Induced Plasticity) steel was investigated by means of microstructural observation and computer modeling. Studies were made on each of three stages of the continuous annealing process applied to TRIP steel. Ortho-equilibrium partitioning of alloying elements of Si and Mn was attained even in short intercritical annealing time. A transformation model, in which transformation is controlled by carbon diffusion, well described the volume fractional change of ferrite and pearlite during the cooling to austempering temperature. Slower cooling rates significantly increased carbon concentration enriched in untransformed austenite and caused pearlite transformation. Ultimate bainite volume fraction obtained by austempering increased with austempering temperature. Analysis with computer modeling revealed that transformation kinetics above 350°C followed a model based on the diffusional mechanism, while it complied with a model based on the displacive mechanism below 350°C.

Precipitation and growth of γ' phase in an Fe-38Ni-13Co-4.7Nb superalloy

K. KUSABIRAKI et al.

An Fe-38Ni-13Co-4.7Nb base superalloy (alloy 909) is the latest low thermal expansion chromium-free superalloy with a good resistance to SAGBO (Stress Accelerated Grain

Boundary Oxidation) embrittlement at elevated temperatures. This investigation is carried out to elucidate the relation between the age-hardening and the nucleation and growth behavior of γ' precipitates in alloy 909 by micro-Vickers hardness test and transmission electron microscopy. The hardness of alloy 909 measured at aging temperatures is ca. HV100 lower than that measured at room temperature. The hardness of specimen aged at 893-1033 K for durations up to 720 ks closely relates to the mean size of γ' precipitates. The growth kinetics of the γ' precipitates in ϵ phase free region is explained by Lifshitz-Slyozov-Wagner's theory of volume diffusion controlled growth at 943-1033 K. The activation energy for the growth of γ' precipitates is estimated to be 254 kJ/mol which is nearly equal to those of diffusion of Ti or Fe atoms in γ -iron or nickel.

Physical and Mechanical Properties

Plastic zones formation under different types of loading conditions

G. V. KLEVTSOV et al.

The plastic zone formation under the fracture surface in materials possessing a Body-Centered Cubic Lattice (BCC) structure (steel 20, 40, 45, St3, 15X2M ϕ A) and materials possessing a Face-Centered Cubic Lattice (FCC) structure (aluminium alloy D16 and austenitic steels 40Г18 ϕ , 40X4Г18 ϕ , 03X13AГ19, 07X13H4AГ20) was studied by the X-Ray Diffraction method. Specimens were tested under a static, impact, high-speed impulse, cyclic (fatigue) and impact-cyclic loading condition at the wide temperature range.

It was shown that two plastic zones were formed under all above types of loading conditions if the plane stress state was attained at the crack tip. Only one micro-plastic zone is formed under the plane strain deformation state.

A scheme of two plastic zones formation at the crack tip of specimens tested under a static, impact and impulse types of loading conditions is presented.

Besides that, it was found that both impulse and impact-cyclic loadings resulted in not only plastic zones formation but work hardening of the material of specimens.

X-ray diffraction technique for analysing failed components

G. V. KLEVTSOV et al.

General criteria for determination the local stress state at the crack tip of the material under different types of loading conditions such as: i) static, ii) impact, iii) high-speed impulse, iv) impact-cyclic, v) cyclic are proposed. They are the ratio of the maximum depth plastic zone to the specimen thickness (h_{max}/t) and the ratio of the diffraction line